

# LHC Implications of the WIMP Miracle and Grand Unification

Can Kılıç,<sup>1</sup> Karoline Köpp,<sup>2</sup> and Takemichi Okui<sup>2</sup>

<sup>1</sup>*Department of Physics and Astronomy, Rutgers University, Piscataway, NJ 08854, USA*

<sup>2</sup>*Department of Physics, Florida State University, Tallahassee, FL 32306, USA*

With the assumptions that dark matter consists of an electroweak triplet and that the gauge couplings unify at a high scale, we identify robust phenomenological trends of possible matter contents at the TeV scale. In particular, we expect new colored states within the LHC reach that can have Yukawa couplings  $\lambda$  to quarks and the Higgs. We investigate the collider signatures that are characteristic of all such models by adopting the model with the simplest matter content as a benchmark. The  $\lambda$  couplings are constrained by flavor/ $CP$  physics. In the largest portion of the allowed parameter space the new colored particles are stable on collider time scales, hence appearing as R-hadrons, for which there is discovery potential at the *early* LHC ( $\sqrt{s} = 7$  TeV,  $1 \text{ fb}^{-1}$ ). Flavor/ $CP$  constraints nevertheless do allow a sizable range of  $\lambda$  where the new colored particles decay promptly, providing a new Higgs production channel with a cross-section governed by the *strong* interaction. Studying the case of  $h \rightarrow WW$ , we show that it is possible for the Higgs production from this new channel to be discovered before that from the Standard Model at the LHC.

## I. INTRODUCTION

The existence of dark matter (DM) is arguably the most compelling evidence for new physics beyond the standard model (SM). Even though existing data provides little insight into the identity and nature of the DM particle, a simple and robust candidate is provided by a weakly interacting massive particle (WIMP), as its relic abundance will be automatically of the right size when its mass is at the TeV scale (“the WIMP miracle”). Since the null results from direct DM search experiments have excluded a WIMP with nonzero hypercharge [1], the simplest WIMP DM candidate is an  $SU(2)_L$ -triplet with  $Y = 0$ , denoted as a  $V$  hereafter. The  $V$  can be made stable by imposing e.g. the  $\mathbb{Z}_2$  parity  $V \rightarrow -V$ . A careful calculation of the relic abundance of a  $V$  is performed in Ref. [2], including non-perturbative effects and possible co-annihilations, finding that the  $V$  mass should be 2.5 TeV if the  $V$  is spin-0, or 2.7 TeV if spin-1/2, assuming that the  $V$  accounts for the entire missing mass of the universe.

Unfortunately, since the  $V$  is heavy and color-neutral, it is virtually impossible to be directly produced from  $pp$  collisions at the Large Hadron Collider (LHC). However,  $V$  may well be part of a bigger, well-motivated extension of the SM containing other new particles that can give rise to observable LHC signals.

In this paper, we adopt gauge coupling unification [3] as a guiding principle besides WIMP DM. Although this is still not constraining enough to point to one single model, it is possible to identify generic, robust phenomenological trends in such extensions of the SM. Concretely, we adopt the  $V$  as a dark matter candidate and demand perturbative gauge coupling unification.<sup>1</sup> We

assume no extra mass scales other than the unification scale and the TeV scale dictated by the WIMP miracle. Finally, we assume that new particles, including the  $V$ , are all fermions to avoid extra fine-tuning problems associated with scalar masses. These assumptions readily imply the existence of additional new particles at the TeV scale, since the gauge couplings in the SM+ $V$  theory do not unify. In particular, we find that there must exist new colored particles at the TeV scale. We also find that the new colored particles generically allow Yukawa couplings to quarks and the Higgs.

Split supersymmetry [4, 5] is a well-studied scenario also based on WIMP DM and gauge coupling unification, as well as the absence of supersymmetry at the TeV scale as in our scenario. There are two major differences. First, contrary to one of our assumptions above, split supersymmetry has an extra threshold between the TeV and unification scales, where we have all the squarks and sleptons, and most importantly, the second Higgs doublet, which affects unification. Second, in split supersymmetry, WIMP DM has to be a nontrivial composition of the higgsinos, wino and/or bino; if we assume that dark matter in split supersymmetry is a pure wino (i.e. the  $V$ ) as in our scenario, gauge coupling unification would not work well (using the same criteria for precision as we use in Sec. II) unless we have a hierarchy larger than two orders-of-magnitude between the higgsino and gluino masses.

The existence of new colored particles with Yukawa couplings  $\lambda$  to quarks and the Higgs suggests the following two scenarios for the LHC. If  $\lambda$  is sufficiently small, the new colored particles will be collider stable, appearing as massive stable hadrons (“R-hadrons”). Since R-hadron signals can be quite spectacular, this is an exciting possibility already for the *early* LHC run at

<sup>1</sup> Note that a  $V$  is not only the simplest WIMP DM candidate of all but also the only  $SU(2)_L$  multiplet with zero hypercharge

that appears within simple  $SU(5)$  multiplets, **5**, **10**, **15**, and **24**.

$\sqrt{s} = 7$  TeV with an integrated luminosity  $\approx 1 \text{ fb}^{-1}$ . On the other hand, if  $\lambda$  is not so small, the new colored particles will decay promptly via  $\lambda$ , with an  $\mathcal{O}(1)$  fraction of their decays containing Higgs bosons. This is an interesting new production channel for the Higgs boson, where the size of the cross-section is governed by the *strong* interaction, potentially making the LHC a ‘‘Higgs factory’’.

To perform quantitative benchmark studies of these characteristic phenomenological features of WIMP DM and unification, we choose as a simple benchmark model consisting of a DM candidate  $V$  and new colored particles  $X$  (to be specified more explicitly later). Among all models with WIMP DM and unification, this benchmark model contains the smallest number of new multiplets beyond the SM, but it already exhibits the two classes of generic collider signatures mentioned above.

Our analysis on this benchmark model will show that, for the range  $m_X = 360\text{--}650$  GeV, the early LHC phase (7 TeV,  $1 \text{ fb}^{-1}$ ) should have sufficient discovery potential for the R-hadron case. For the Higgs factory case, we will lay out an experimental strategy for the full LHC at  $\sqrt{s} = 14$  TeV. This consists of two parts, the discovery of the  $X$  and measurement of  $m_X$ , and the discovery of the Higgs bosons from the  $X$  decays. We will show that with  $10 \text{ fb}^{-1}$  of data at the LHC (14 TeV), it should be possible to discover the  $X$  and the Higgs bosons from the  $X$  decays in the range  $300 < m_X \lesssim 550$  GeV for a moderately heavy Higgs (i.e. decaying to weak gauge bosons).

This paper is organized as follows. In Sec. II we survey possible extensions of the SM that feature gauge coupling unification and WIMP DM. In Sec. III we describe our simple benchmark model that phenomenologically represents all such extensions. The couplings  $\lambda$  of the new colored particles to quarks and the Higgs are expected to have an upper bound from flavor/ $CP$ /electroweak constraints, which is analyzed in Sec. IV using the benchmark model. The collider signatures of the R-Hadron case and the Higgs factory case are studied in detail in Sec. V A and Sec. V B, respectively. In Sec. VI we summarize our analyses and indicate some possible future directions. In Appendix A we discuss how proton decay can be avoided in the class of models we consider in this paper. In Appendix B we comment that the addition of higher-dimensional operators to our Lagrangian does not have any impact on our analysis.

## II. EXTENSIONS OF THE SM FEATURING WIMP DM AND COUPLING UNIFICATION

In this section we enumerate possible extensions of the SM that contain the WIMP DM candidate  $V$  and are consistent with gauge coupling unification, and identify generic features shared by such extensions. This analysis will serve as a basis for our choice of a benchmark model in Sec. III.

Let us assume unification of the SM gauge group into a simple group (such as  $SU(5)$ ) to fix the normalization of hypercharge. The DM candidate  $V$  can be embedded into a  $\mathbf{24}$  of  $SU(5)$ , consistent with this assumption. Moreover, let us assume that all new particles, including the  $V$ , are spin-1/2 fermions in order to avoid unnecessary extra fine-tuning problems associated with scalar masses besides the notorious existing problem with the Higgs mass. As calculated in Ref. [2], the fermionic  $V$  mass is fixed by the relic abundance to be  $m_V = 2.7$  TeV, which we will assume to be the case hereafter.

This cannot be the end of the story, however, because the SM augmented by only the  $V$  is not consistent with gauge coupling unification. There must be additional new particles. In principle, these additional particles could appear anywhere below the unification scale. However, since we must presume some underlying dynamics that generates the TeV scale in order for the WIMP miracle not to be a mere coincidence, we adopt the simplest assumption that the same dynamics also provides TeV-scale masses to the additional new particles, with no extra mass scale other than the TeV scale and the unification scale. We take the new fermions to be vectorlike, because chiral fermions would require electroweak symmetry breaking to acquire TeV-scale masses, which would generically lead to dangerously large corrections to precision electroweak observables, in particular the  $\rho$  parameter [6]. Let us further restrict ourselves to the case where the vectorlike fermions can be embedded into the simplest  $SU(5)$  multiplets,  $\mathbf{5} \oplus \bar{\mathbf{5}}$ ,  $\mathbf{10} \oplus \bar{\mathbf{10}}$ ,  $\mathbf{15} \oplus \bar{\mathbf{15}}$  and  $\mathbf{24}$ . Thus, we consider

$$\begin{aligned} Q &\sim (\mathbf{3}, \mathbf{2})_{1/6}, & U &\sim (\mathbf{3}, \mathbf{1})_{2/3}, & D &\sim (\mathbf{3}, \mathbf{1})_{-1/3}, \\ L &\sim (\mathbf{1}, \mathbf{2})_{-1/2}, & E &\sim (\mathbf{1}, \mathbf{1})_{-1}, & X &\sim (\mathbf{3}, \mathbf{2})_{-5/6}, \\ S &\sim (\mathbf{6}, \mathbf{1})_{-2/3}, & T &\sim (\mathbf{1}, \mathbf{3})_1, & V &\sim (\mathbf{1}, \mathbf{3})_0, \\ G &\sim (\mathbf{8}, \mathbf{1})_0, \end{aligned}$$

as well as the conjugates  $Q^c, U^c, \dots, T^c$ , except for  $V$  and  $G$ , which are real. (Our convention is such that  $H$  has the quantum numbers  $(\mathbf{1}, \mathbf{2})_{1/2}$ . The SM fermions are denoted by lower-case letters,  $q, u^c, d^c, \ell, e^c$ .) As we will see below, this already provides a sufficient number of candidate models for us to observe generic trends in extensions of the SM with WIMP DM and gauge coupling unification.

In searching for possible field contents that can lead to unification, there are various uncertainties that must be taken into account when we ‘‘predict’’ the  $SU(3)_C$  coupling  $\alpha_3$  in terms of  $\alpha_{1,2}$ , which we regard as precise. First, in our RG analysis, which we perform at the 1-loop level, there is a threshold ambiguity at  $m_V = 2.7$  TeV. We estimate this uncertainty by varying the  $\overline{\text{MS}}$  subtraction scale  $\mu$  from  $m_V/\sqrt{2}$  to  $\sqrt{2}m_V$ . Second, unlike the  $V$  mass, the masses of the additional fermions cannot be fixed a priori and can be anywhere at the TeV scale, from a few hundred GeV to several TeV. Therefore, we scan over the additional fermions’ masses in the range between 300 GeV and 10 TeV, where for simplicity we

$2X$	$2X + D + L$	$2U + T + E$
$U + S + 2T$	$2X + 2U + T$	$3X + L + E$
$3X + G + V$	$3U + T + L$	$\dots$

TABLE I: Possible combinations of new fermions that, together with the DM  $V$ , could lead to unification. It is understood that the new fermions are vectorlike, so in writing  $X$ ,  $U$ ,  $\dots$ , the presence of their charge conjugates  $X^c$ ,  $U^c$ ,  $\dots$  is also implied, except for the Majorana fermions  $V$  and  $G$ .

assume a single common mass for all of them.<sup>2</sup> These two sources of uncertainty each shift our  $\alpha_3$  prediction at the level of a few times  $\Delta\alpha_3^{(\text{exp})}$ ; the experimental uncertainty in the measurement  $\alpha_3^{(\text{exp})} = 0.1184 \pm 0.0007$  [7]. We demand that the “band” in our  $\alpha_3$  prediction combining these two uncertainties have an overlap with the band corresponding to  $3\Delta\alpha_3^{(\text{exp})}$  (i.e.  $3\sigma$ ). There are also threshold effects from unspecified GUT physics, but we assume that they are similar in size to the uncertainties mentioned above and simply neglect them. Finally, we demand that the coupling at the unification scale be perturbative,  $\alpha_{\text{GUT}} < 1$ .

A similar analysis was performed in Ref. [5], where the main difference lies in the treatment of proton decay. While Ref. [5] demands the unification scale to be higher than  $\sim 10^{16}$  GeV in order to sufficiently suppress proton decay, we choose to impose a symmetry to forbid proton decay, and only demand the GUT scale to be higher than  $10^5$  TeV (and lower than the Planck scale  $\sim 10^{18}$  GeV) to avoid having to address possible conflicts between GUT physics and flavor/ $CP$  bounds. The use of a symmetry to forbid proton decay requires some model building at the unification scale, but it has no observational consequences for the TeV-scale physics, so we leave the model building to Appendix A. Another difference between our analysis and that of Ref. [5] is that in calculating the running of the gauge couplings, Ref. [5] assumes that all new particles have masses near  $m_Z$ , while our masses span a wide range around a TeV, as we described above.

There are 22 models satisfying the above criteria with no more than 3 types of multiplets in addition to the  $V$  and no more than 3 generations per type. Particularly simple ones are listed in Table I. All the 22 models share the following features:

- (1) There exist new colored particles.
- (2) The quantum numbers of these new colored particles allow Yukawa couplings to quarks and the Higgs.

Property (1) is clearly favorable for hadron colliders. Even better, all the 22 models actually survive even if

<sup>2</sup> New charged/colored particles below 300 GeV are likely to be already excluded, as will be illustrated by the analysis of the benchmark model below.

we restrict the additional fermions’ masses to the range 300 GeV-1 TeV, so they all can be potentially within the LHC reach. Property (2) is not satisfied by  $S$  and  $G$ , but they only appear twice each among the 22 models, and even those models contain other colored particles that do satisfy property (2). We therefore identify these properties as robust LHC implications of WIMP DM and unification.<sup>3</sup>

To assess the robustness of the above features further, one can repeat the exercise with more conservative estimates on the uncertainties in the prediction of  $\alpha_3$ . For example, if we vary the matching scale  $\mu$  from  $m_V/2$  to  $2m_V$  (with everything else treated as above), we obtain 63 models, of which there is only one model ( $V + E$ ) without colored particles,<sup>4</sup> and only 6 colored models without property (2). Again, most models survive even if we restrict the search in the “LHC-accessible” range 300 GeV-1 TeV; 44 models in total, only one colorless model, and only one colorful model without property (2).

In the next section, we choose a benchmark model that represents characteristic phenomenologies of all these models which follow from properties (1) and (2). We will then use the benchmark model for further, more quantitative analyses in later sections.

### III. THE BENCHMARK MODEL

Given the insights from Sec. II, we select the model with the dark matter  $V$  and two generations of  $X \oplus X^c$  as our benchmark. This is the simplest of all models with a  $V$  featuring unification, having the smallest number of new multiplets beyond the SM. But most importantly, the collider phenomenology of this model is representative of all models identified in Sec. II as far as the LHC phenomenology is concerned.

The most general renormalizable Lagrangian for the  $2X + V$  model consistent with the  $\mathbb{Z}_2$  symmetry  $V \rightarrow -V$  reads

$$\begin{aligned} \mathcal{L} = & \mathcal{L}_{\text{SM}} + \bar{V}\sigma^\mu iD_\mu V - \frac{m_V}{2}VV \\ & + \sum_a \left[ \bar{X}_a \bar{\sigma}^\mu iD_\mu X_a + X_a^c \sigma^\mu iD_\mu \bar{X}_a^c \right. \\ & \left. - \left( m_{X_a} X_a^c X_a + \sum_i \lambda_{ia} H d_i^c X_a + \text{c.c.} \right) \right], \end{aligned} \quad (1)$$

where  $a = 1, 2$  and  $i = 1, 2, 3$  denote generations of the  $X$  and  $d$ -type quark, respectively. We also use  $X_{-1/3}$

<sup>3</sup> Recall the crucial role of the WIMP miracle in selecting the TeV scale as the mass scale for the new particles.

<sup>4</sup> Actually, a closer inspection reveals that unification favors the  $E$  in the  $V + E$  model to be lighter than  $\approx 300$  GeV. The quantum numbers of the  $E$  allow it to decay to  $\ell + Z$  in particular, so this model is already excluded.

and  $X_{-4/3}$  to refer to the upper and lower  $SU(2)_L$  components of  $X$ , respectively, where the subscripts denote the electric charges.

It is technically natural for  $\lambda$  to take any value, but there are obvious phenomenological constraints. First,  $\lambda$  has to be nonzero because the  $X$ s must eventually decay to avoid cosmological problems. (However, the  $X$ s could decay via higher dimensional operators. See Appendix B). Second,  $\lambda$  must be much less than  $\mathcal{O}(1)$  because  $\lambda$  breaks the  $U(3)^5$  flavor symmetry of the SM, providing new sources of flavor/ $CP$  violations in addition to the SM Yukawa couplings. We will return to flavor/ $CP$  constraints in Sec. IV.

The leading decays of  $X$  induced by  $\lambda$  can be most easily understood by the Goldstone equivalence theorem. In the limit of keeping only the  $X$  mass, the equivalence theorem tells us that  $X_{-1/3}$  will decay as

$$X_{-1/3} \rightarrow Z + d, \quad X_{-1/3} \rightarrow h + d \quad (2)$$

with equal probabilities, where  $d$  can be any down-type quark.<sup>5</sup> Note that the equivalence theorem holds only in this limit. When the finite masses of the Higgs and  $Z$  bosons are taken into account, the branching fraction for the  $Z$  channel is expected to be somewhat larger due to phase space. For low  $X$  masses and/or a heavy Higgs, this can have a significant impact on the phenomenology. Similarly,  $X_{-4/3}$  can decay as

$$X_{-4/3} \rightarrow W^- + d, \quad (3)$$

which will be the dominant decay mode as long as the corresponding rate can be regarded as prompt on the collider time scale. When this rate drops below the displaced-vertex range, the dominant decay of the  $X_{-4/3}$  will be through the weak interaction to an  $X_{-1/3}$ , which becomes slightly lighter than  $X_{-4/3}$  after electroweak symmetry breaking, as we will elaborate more in Sec. V A.

Therefore, depending on the size of  $\lambda$ , we have either of the following collider signatures:

- (A) If  $\lambda$  is sufficiently tiny, the  $X$  will be stable on collider time scales, and upon production it will hadronize into stable massive hadrons (“R-hadrons”). R-hadrons are easy to observe when they are charged, so  $X$  may be discoverable already in the early LHC run (i.e. 7 TeV, 1 fb<sup>-1</sup>).
- (B) If  $\lambda$  is not so small (but small enough to satisfy flavor/ $CP$  constraints), the  $X$  will decay within the detector, and as we have seen above, roughly a quarter of  $X$ s (a half of  $X_{-1/3}$ s) will decay to a

Higgs boson (plus a jet). This is an exciting possibility — a “Higgs factory” — where the Higgs bosons are produced with a characteristic  $2 \rightarrow 2$  cross-section of the *strong* interaction. In the remaining 3/4 of the time, the  $X$  will decay to a  $Z$  or  $W$  boson. Then, leptonic  $Z$  decays can be used to discover the  $X$  itself.

In Sec. IV we will show that flavor/ $CP$  constraints indeed allow a window for the case (B).

Note that possibilities (A) and (B) are common to all the 22 models identified in Sec. II. For example, in models containing  $Q$  instead of  $X$ , the  $\lambda$  coupling in Eq. (1) should be replaced by  $\lambda_u H u^c Q + \lambda_d H^* d^c Q$ , which would exhibit the same phenomenology as above. In models containing  $U$  or  $D$  instead of  $X$ , the  $\lambda$  coupling is replaced by  $\lambda H U^c q$  and  $\lambda H^* D^c q$ , respectively, which is again phenomenologically equivalent.

Actually, the models with  $Q$ ,  $U$  and/or  $D$  have additional potentially interesting modes  $Q \rightarrow Z + t$ ,  $Q \rightarrow W + t$ ,  $U \rightarrow Z + t$ , or  $D \rightarrow W + t$ . While the appearance of the top constitutes a qualitative difference in the collider phenomenology, a full analysis for such decay channels is more complicated due to the higher final-state multiplicity from the top decay. There are reducible background sources which cannot be simulated reliably at the matrix element level due to the large number of final-state particles, and even for irreducible backgrounds the issue of combinatoric backgrounds makes searches more difficult. Some of these problems may be ameliorated if an  $\mathcal{O}(1)$  fraction of tops is produced with large  $p_T$ , such that the recently developed methods of boosted top-tagging [8] can be applied. We will leave these more complicated cases to future work and focus in this paper on the phenomenology of signatures (A) and (B).

#### IV. FLAVOR/ $CP$ AND ELECTROWEAK CONSTRAINTS

In this section, we analyze flavor/ $CP$  violations as well as corrections to precision electroweak observables in the benchmark model. These corrections arise due to the coupling

$$\mathcal{L} \supset \lambda_{ia} H d_i^c X_a + \text{c.c.}, \quad (4)$$

where  $a = 1, 2$  and  $i = 1, 2, 3$ . We will adopt the most conservative assumption that  $\lambda$  is an “anarchic” matrix without any special texture or alignment:

$$(\lambda_{ia}) = \begin{pmatrix} \sim \lambda & \sim \lambda \\ \sim \lambda & \sim \lambda \\ \sim \lambda & \sim \lambda \end{pmatrix}. \quad (5)$$

Therefore, the bounds discussed in this section could be relaxed by further model building or extra assumptions on the structure of  $\lambda$ . (For example, Ref. [9] introduces a model with a single  $X$  particle (and no  $V$ )

<sup>5</sup> The small violation of the equivalence theorem induces additional decays such as  $X_{-1/3} \rightarrow W^- + u$ , which can be thought of as arising from mixing of the  $X$ s with down-type quarks. However, as we will see in Sec. IV, flavor/ $CP$  bounds constrain such mixings to be tiny, rendering these decay modes negligible.



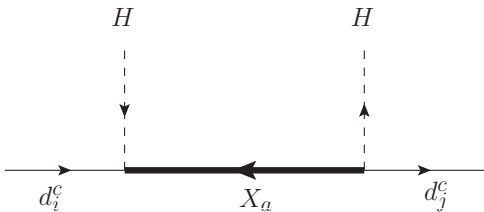


FIG. 1: Diagram leading to the operator (6).

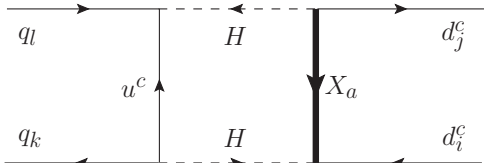


FIG. 2: Diagram leading to the four fermion operator (8).

with a similar coupling selectively to the third generation, and consequently their model is much less constrained by flavor/ $CP$ .)

Since the  $X$ s are heavier than all SM particles and we anticipate a small  $\lambda$ , we integrate out the  $X$ s and analyze effective operators in powers of  $\lambda/m_X$ . Strictly speaking, the ratio  $\langle H \rangle/m_X$  is not a very small number, so contributions higher order in  $\langle H \rangle/m_X$  can change our estimates by an  $\mathcal{O}(1)$  factor. However, our interest is to show that a robust ‘‘Higgs factory’’ window can exist for the broad scenario of extending the SM with WIMP DM and unification, rather than placing precise bounds on this particular benchmark model. Therefore, order-of-magnitude estimates suffice for this purpose.

The most stringent bound comes from  $K^0-\bar{K}^0$  mixing. The relevant tree and 1-loop diagrams are shown in Figs. 1 and 2, respectively. Upon integrating out  $X$  in Fig. 1, we generate the operator

$$\sum_{i,j,a} \frac{\lambda_{ia}\lambda_{aj}^\dagger}{m_{X_a}^2} d_i^c \sigma^\mu \bar{d}_j^c (H^\dagger \overleftrightarrow{D}_\mu H). \quad (6)$$

Below the  $Z$  mass, using this operator twice with all the four  $H$ s put to VEVs would generate 4-fermion operators with four right-handed down-type quarks with a coefficient  $\sim \lambda^4 v^2/m_X^4$ , which is conservatively  $\sim \lambda^4/m_X^2$ . In particular, the imaginary part of the coefficient of  $(d^c \sigma_\mu \bar{s}^c)(\bar{d}^c \sigma^\mu s^c)$  is constrained and has to be less than  $(10^4 \text{ TeV})^{-2}$  [10]. With our assumption of anarchic  $\lambda$ , we expect an  $\mathcal{O}(1)$  phase in  $\lambda^4$ , so we obtain the bound

$$\lambda \lesssim 10^{-2} \sqrt{\frac{m_X}{1 \text{ TeV}}}. \quad (7)$$

Similarly, upon integrating out  $X$  in Fig. 2, we generate the operator

$$\sim \frac{1}{16\pi^2} \sum_{a,i,j,k,\ell} \frac{\lambda_{ia}\lambda_{aj}^\dagger (y_u^\dagger y_u)_{k\ell}}{m_{X_a}^2} (d_i^c \sigma_\mu \bar{d}_j^c) (\bar{q}_k \bar{\sigma}^\mu q_\ell). \quad (8)$$

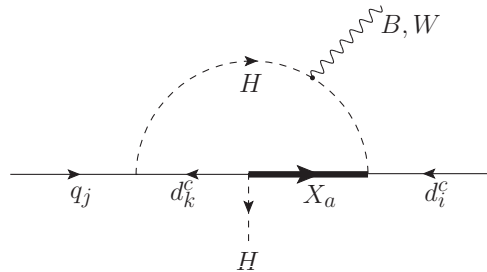


FIG. 3: One of the diagrams leading to the dipole operator (11).

From this, the imaginary part of the coefficient of  $(d^c \sigma_\mu \bar{s}^c)(\bar{d}^c \sigma^\mu s^c)$  can be estimated to be

$$\sim \frac{1}{16\pi^2} \frac{\lambda^2 \theta_c^5}{m_X^2}, \quad (9)$$

where we have used  $(y_u^\dagger y_u)_{12} \sim y_t^2 \theta_c^5 \approx \theta_c^5$  with the Cabibbo angle  $\theta_c \approx 1/5$ . This coefficient should be less than  $(10^5 \text{ TeV})^{-2}$  [10], which implies

$$\lambda \lesssim 10^{-2} \frac{m_X}{1 \text{ TeV}}. \quad (10)$$

The bound (10) is slightly stronger than the bound (7) for  $m_X \lesssim 1 \text{ TeV}$ , so we adopt Eq. (10) as our upper bound on  $\lambda$ .

No other constraints are as strong as Eq. (10). For example, let us look at the dipole operators generated from diagrams as in Fig. 3:

$$\sim \frac{g_F}{16\pi^2} \sum_{a,i,j,k} \frac{\lambda_{ia}\lambda_{ak}^\dagger (y_d)_{kj}}{m_{X_a}^2} H^\dagger d_i^c \bar{\sigma}^{\mu\nu} F_{\mu\nu} q_j, \quad (11)$$

where  $F = B, W$  denotes the electroweak gauge fields, which in particular contribute to  $b \rightarrow s\gamma$  after electroweak symmetry breaking. Since these operators are suppressed by the small bottom Yukawa coupling  $y_b \sim 1/40$ , one can think of them as the  $b \rightarrow s\gamma$  dipole operator in minimal flavor violation [11] with the scale  $\Lambda \sim 4\pi\theta_c m_X / (\sqrt{e}\lambda)$ , where  $e$  is the QED coupling. Then, the bound  $\Lambda \sim 10 \text{ TeV}$  from  $b \rightarrow s\gamma$  [11, 12] implies  $\lambda/m_X \lesssim 10^{-1} \text{ TeV}^{-1}$ , which is again weaker than Eq. (10).

Let us also look at precision electroweak constraints. First, the operator (6) modifies  $Z \rightarrow b\bar{b}$ :

$$\frac{\Delta g_{Zb\bar{b}}}{g_{Zb\bar{b}}} \sim \frac{\lambda^2}{m_X^2}. \quad (12)$$

Again, given Eq. (10), this is safely below the experimental bound.<sup>6</sup> Second, Fig. 4 generates an operator

<sup>6</sup> Ref. [9] discusses a model with a single generation of  $X$  (and without  $V$ ), in which they exploit this shift in  $Z \rightarrow b\bar{b}$  to improve precision electroweak fits of the SM.

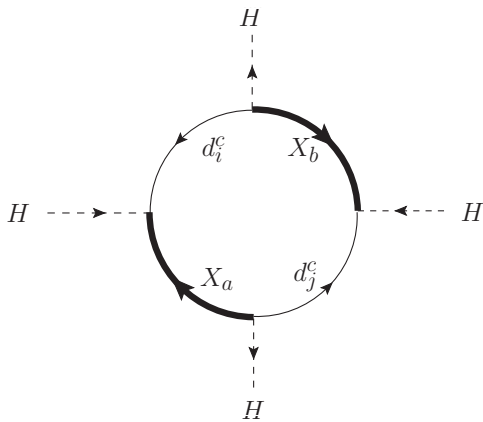


FIG. 4: Diagram contributing to the  $\rho$  parameter (13).

contributing the  $\rho$  parameter

$$\sim \frac{\lambda^4}{16\pi^2 m_X^2} (H^\dagger D_\mu H)(H^\dagger D^\mu H). \quad (13)$$

The coefficient should be less than  $\sim 10^{-3}/v^2$  [13] with  $v = 174$  GeV, implying  $\lambda \lesssim \sqrt{m_X}/(1 \text{ TeV})$ , which again is much weaker than Eq. (10).

Given the bound (10), there is clearly a robust ‘‘Higgs factory’’ window where the  $X$ s decay promptly. Keeping only the  $X$  mass for simplicity, the decay rate of an  $X$  via coupling (4) is given by  $\Gamma_X \sim \lambda^2 m_X/16\pi$ . Therefore, demanding  $\Gamma_X^{-1} \lesssim 10^{-12}$  s (i.e. the decay length shorter than  $\mathcal{O}(0.1)$  mm), we obtain the Higgs-factory window

$$10^{-7} \left( \frac{1 \text{ TeV}}{m_X} \right)^{\frac{1}{2}} \lesssim \lambda \lesssim 10^{-2} \frac{m_X}{1 \text{ TeV}}. \quad (14)$$

Below the Higgs-factory window, there is a two or three orders-of-magnitude window where an  $X$  decays with a displaced vertex or in the LHC detector but with a macroscopic decay length. At a hadron collider, events where new physics only manifests itself at a macroscopic distance from the interaction point but still within the volume of the detector are challenging. Such signatures also appear in supersymmetric theories [14, 15], hidden valley models [16], quirk models [17], and vector-like confinement models [18]. As discussed in section 16 of Ref. [19] (and references therein), when particles with macroscopic decay lengths are produced, trigger efficiencies can become a concern. Recently, the prospects of a similar final state from late-decaying neutralinos in a supersymmetric model have been carefully studied in Ref. [20], with encouraging results. While the case of macroscopic decay lengths is interesting, the subtleties involved require a study with a more sophisticated detector simulation than PGS [21] (which we use in our analysis). In addition, it is possible for R-hadrons to stop in the detector [22]. These are important questions worth investigating in detail, which we leave to future work.

## V. COLLIDER PHENOMENOLOGY

In this section we will investigate in detail the two characteristic collider signatures of our scenario using the benchmark model. When the  $X$ s are collider stable, we will show that the discovery of  $X$  is possible up to  $m_X = 650$  GeV in the early 7-TeV run with  $1 \text{ fb}^{-1}$  of data, and well past 1 TeV with the 14-TeV running. When the  $X$ s decay promptly, we will concentrate on the discovery of the  $X$  and the Higgs bosons from  $X$  decays for early 14-TeV running ( $10 \text{ fb}^{-1}$ ). In order to keep the analysis simple, we will restrict ourselves to the case of a moderately heavy Higgs ( $m_h = 200$  GeV), but we expect the Higgs discovery potential to be similarly enhanced for a light Higgs as well.

Even though the benchmark model contains two generations of  $X$ , we have no reason to expect that they would be exactly degenerate in mass. Since the production cross-section will be dominated by the lighter  $X$ , we will base our collider analysis on one generation of  $X$  only. This is the most conservative choice; if the  $X$ s do happen to be nearly degenerate, this would significantly enhance the results below.

### A. R-hadron Signals at the LHC

When the coupling  $\lambda$  is sufficiently small, the  $X$  does not decay within the detector. The signature therefore is that of an ‘‘R-hadron’’, that is, the  $X$  hadronizes with light colored degrees of freedom and the color-neutral bound state behaves as a (possibly charged) stable massive particle. Before we present a quantitative analysis, let us dwell on a few qualitative features of this signature.

Firstly, note that even when  $\lambda$  is very small,  $X_{-4/3}$  still decays to  $X_{-1/3}$  via the weak interactions, and in terms of collider signatures, the production of  $X_{-4/3}$  is indistinguishable from that of  $X_{-1/3}$  because the decay products are virtually unobservable. As worked out in detail in Ref. [23],  $X_{-4/3}$  is expected to be heavier than  $X_{-1/3}$  by only  $\Delta m_X = 0.60$  GeV. The dominant decay mode is  $X_{-4/3} \rightarrow X_{-1/3} + \pi^-$  through an off-shell  $W^-$ , with a partial width

$$\Gamma^{-1} = 1.3 \text{ mm} \left( \frac{0.60 \text{ GeV}}{\Delta m_X} \right)^3 \sqrt{\frac{1 - \frac{m_\pi^2}{(0.60 \text{ GeV})^2}}{1 - \frac{m_\pi^2}{\Delta m_X^2}}}. \quad (15)$$

The smallness of the mass gap makes the  $\pi$  very soft and thus unobservable at the LHC, and other subdominant decay modes have the same problem. Therefore, in analyzing the discovery potential or checking existing bounds, the production cross-section of  $X_{-4/3}$  should be added to that of  $X_{-1/3}$ .

The charge of an R-hadron is crucial for prospects of observing it. In particular, the most effective way to trigger on a stable charged massive particle is via the muon system [24]. The bound states of an  $X_{-1/3}$  can

be mesons ( $X\bar{q}$ ) or baryons ( $Xqq$ ). The physics of these bound states can be understood by regarding the  $X_{-1/3}$  as a heavy version of the  $b$  quark, which is already much heavier than  $\Lambda_{\text{QCD}}$ . The lightest  $B$  mesons are  $B^0$  and  $B^\pm$ , with only a few-hundred-keV mass splitting, while the lightest  $B$  baryon  $\Lambda_b^0$  is heavier than the  $B^{0,\pm}$  by 340 MeV. Therefore, we expect that the lightest  $X$ -meson should be lighter than the lightest  $X$ -baryon also by  $\sim 340$  MeV, with a few-hundred-keV mass splitting between the neutral and charged  $X$ -mesons. Since the splitting between the lightest  $X$ -meson and  $X$ -baryon is on the order of  $\Lambda_{\text{QCD}}$  itself, we expect that an  $X$  should preferentially hadronize into an  $X$ -meson, which can be either charged or neutral with 50% probability because their mass difference is tiny.<sup>7</sup>

In order to estimate the trigger efficiencies, we will use the following assumptions in the rest of our analysis:

- There is a 50% chance that an R-hadron is charged when produced at the primary interaction.
- This charge is retained until the calorimeter is reached.
- One or more charge exchange interactions take place in the calorimeter, randomizing the charge of the R-hadron such that there is a 50% chance that it reaches the muon chamber as a charged particle.<sup>8</sup>

One of the requirements for triggering is that the particle reaches the muon system with nonzero charge. Most experimental searches for massive stable particles also use as a selection criterion that there should be a charged track in the inner part of the detector that matches the hit in the muon chamber, even if this is not required for

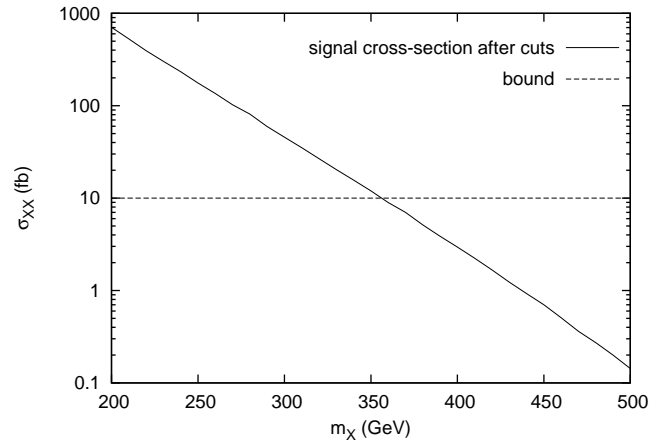


FIG. 5: The cross-section for R-hadron production at the Tevatron after all selection cuts. The bound from the CHAMP search is included for comparison.

triggering. Therefore we will also adopt this as one of our event selection criteria.

Finally, an important kinematic variable, especially at the LHC (where the detectors are physically larger and the time between bunch crossings is short), is the “time-lag”. This is defined as how much later the massive R-hadron ( $\beta < 1$ ) arrives at the muon chamber compared to a relativistic particle (e.g. a muon). To be conservative, we use the physical dimensions of the ATLAS detector (which is larger than CMS) as described in Ref. [24]. Specifically, we differentiate the barrel region ( $|\eta| < 1.4$ ) from the end-cap region ( $1.4 < |\eta| < 2.5$ ). For the barrel region we calculate the time to get to a radius of 7.5 meters from the interaction point, and for the end-cap we calculate the time to get to  $|z| = 14.5$  meters. For the LHC search, we will use as one of the event selection criteria that at least one of the R-hadrons reaches the muon chamber before relativistic particles from the next bunch crossing, i.e., with a time-lag of less than 25 ns.

Before we investigate the discovery potential of  $X$  at the early LHC, let us address constraints on R-hadron production from the Tevatron [26, 27]. We will use the event selection criteria described in Ref. [26] in order to estimate acceptance and trigger rates in the benchmark model. In particular we demand that events contain at least one particle that has  $|\eta| < 0.7$ ,  $p_T > 40$  GeV and  $0.4 < \beta < 0.9$ , leaves a track, and is charged when it arrives at the muon system. For a single R-hadron satisfying these cuts, our above assumptions on the charges of R-hadrons imply a 25% probability for being detected. However, when both of the pair-produced R-hadrons are within acceptance and charged throughout the detector (a 1/16 probability), we need to correct for the fact that the reconstruction and trigger efficiency used in the analysis of Ref. [26] applies to a single R-hadron. Therefore the “effective cross section” for such events needs to be multiplied by a correction factor  $\xi$  before the compari-

<sup>7</sup> The few-hundred-keV mass difference between the  $(X_{-1/3}\bar{d})$  meson and the  $(X_{-1/3}\bar{u})$  meson might allow one to decay to the other via the weak interaction, if the mass difference is larger than the electron mass. But such a decay would occur with an extremely long lifetime (like the  $\beta$ -decay of the neutron), so it can be ignored on collider time scales.

<sup>8</sup> In addition to conversion between the charged and neutral  $X$ -mesons, for which there is a tiny energetic cost of a few hundred keV, there is also a process where an  $X$ -meson scatters into an  $X$ -baryon in the calorimeter [25], which, however, requires an energy of at least  $\sim 340$  MeV. Using the analogy with the  $b$  system, the lightest  $X$ -baryon (analogous to  $\Lambda_b^0$ ) should be neutral, while the lightest charged  $X$ -baryon (analogous to  $\Sigma_b^\pm$ ) should be heavier by  $\sim 190$  MeV. So, a charged  $X$ -baryon, even if produced, would promptly decay to a neutral  $X$ -baryon (by emitting a pion) which would then not be caught by the muon chamber, potentially hurting our R-hadron signal. The question of how frequently this meson-to-baryon conversion occurs is highly nontrivial and beyond the scope of this paper. However, note that a meson-to-baryon conversion would not occur to the  $\bar{X}$  due to the lack of anti-nucleons in the calorimeter. Therefore, even in the worst case where we always lose the R-hadrons from the  $X$ , we still have those from the  $\bar{X}$ , so the effective cross-section would be roughly halved, which would correspond a small shift ( $\sim \mathcal{O}(10)$  GeV) in the mass scale.

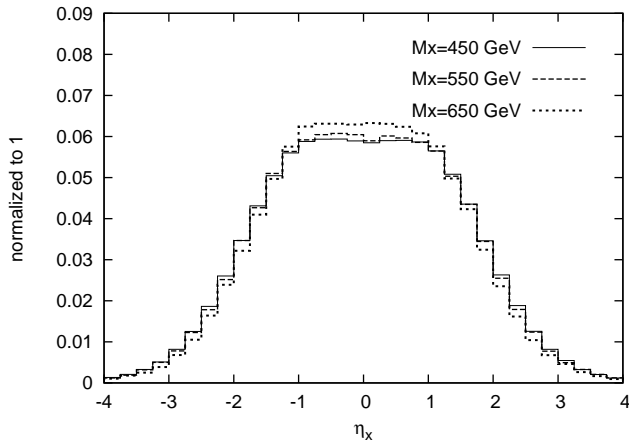


FIG. 6: The rapidity distribution of the R-hadrons at the LHC (7 TeV) for the three mass points.

son with the bound of Ref. [26]. This correction factor is given by  $\xi = (1 - (1 - \epsilon)^2)/\epsilon$ , where  $\epsilon = 0.533$  is the reconstruction efficiency for a single R-hadron [28]. We use `CaLcHEP 2.5.4` [29] with CTEQ6 parton distribution functions [30] to simulate the parton level process. The effective cross-section after the selection cuts is plotted in Fig. 5 against the bound of Ref. [26]. We conclude that  $m_X > 360$  GeV is not excluded.

We now turn to production of R-hadrons at the early LHC, i.e., for the 7-TeV running with  $1 \text{ fb}^{-1}$  of integrated luminosity. We choose to look at mass points  $m_X = 450$  GeV, 550 GeV and 650 GeV. In Fig. 6, we plot the rapidity distribution of the R-hadrons for each mass point to show that R-hadron production is dominantly central. As event selection criteria, we impose that at least one R-hadron must reach the muon detector ( $|\eta| < 2.5$ ) with  $p_T > 30$  GeV and a time lag of less than 25 ns. We further demand that the R-hadron in question leaves a track and is charged when it gets to the muon chamber (a 25% probability per R-hadron as before). In events where both R-hadrons reach the muon chamber with  $p_T > 30$  GeV, we plot the time-lag of the earlier (later) R-hadron in Fig. 7 (Fig. 8). Folding in the time-lag cut and the probability of being charged (but leaving out reconstruction efficiencies, which are unknown at this time), we plot the effective cross-section after all selection cuts in Fig. 9. Note that the efficiency of the selection cuts has a slightly decreasing trend at higher mass, because the production occurs closer to threshold and fewer events satisfy the time-lag cut. Requiring at least 10 events for discovery, we see that  $X$  masses of up to 650 GeV should be within reach with  $1 \text{ fb}^{-1}$  of data from the 7-TeV run.

Using the same selection criteria for the 14-TeV running, we also plot in Fig. 10 the effective cross-section after cuts in that case. We see that even with early 14-TeV data (e.g.  $\approx 10 \text{ fb}^{-1}$ ),  $X$  masses well past 1 TeV should be within reach.

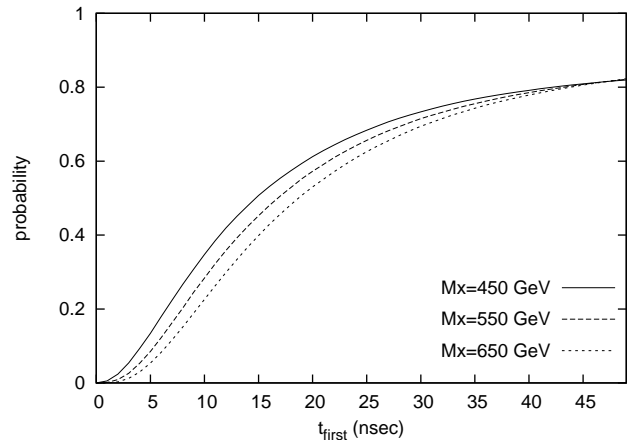


FIG. 7: Time-lag distribution of the first R-hadron to arrive in the muon system at the LHC (7 TeV).

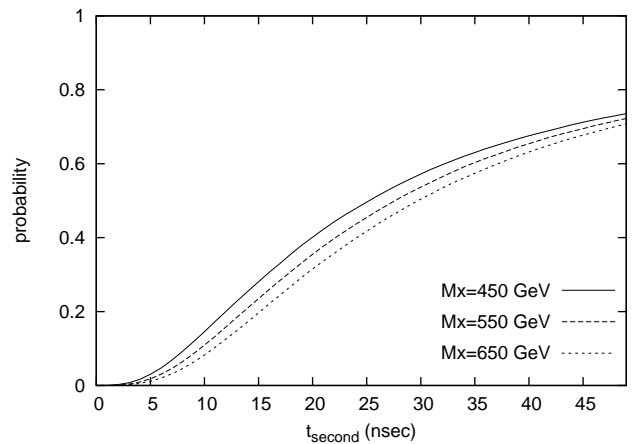


FIG. 8: Time-lag distribution of the second R-hadron to arrive in the muon system at the LHC (7 TeV).

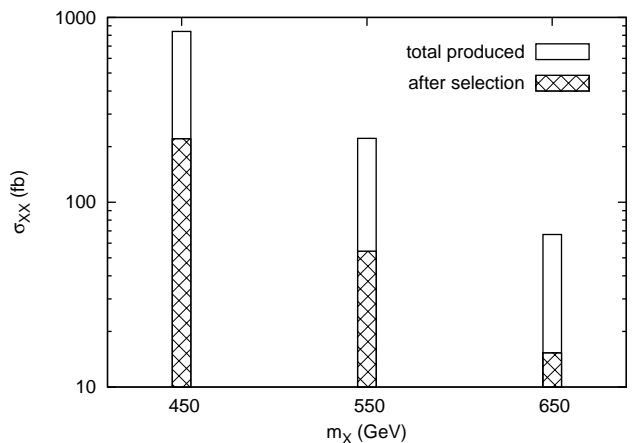


FIG. 9: Total production cross-section of R-hadron production and effective cross-section after selection cuts at the LHC (7 TeV) for the three mass points.



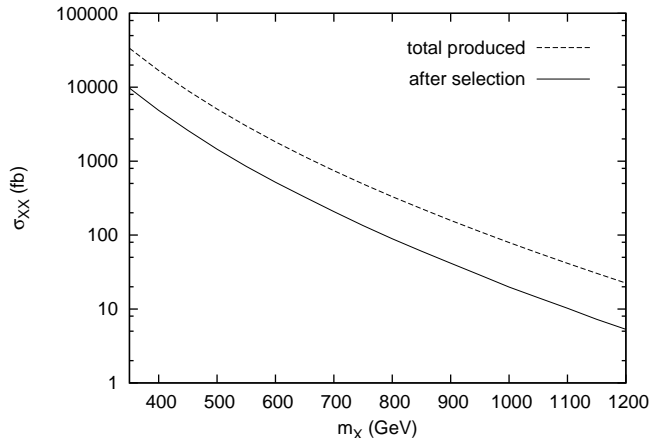


FIG. 10: Effective R-hadron production cross-section after selection cuts at the LHC (14 TeV).

### B. The LHC as a Higgs factory

For  $\lambda$  in the range given by Eq. (14), the  $X$  decays promptly. For the  $X_{-1/3}$ , the dominant decay modes are  $Z + j$  and  $h + j$ . Since production proceeds through QCD, this gives rise to a “Higgs factory” if  $m_X$  is not too large. The  $X_{-4/3}$  decays to  $W + j$  and therefore gives no additional contribution to Higgs production. For the rest of this section, we will be interested in the production of  $X_{-1/3}$  only. We will show that there is a window in  $m_X$ , where with  $10 \text{ fb}^{-1}$  of 14-TeV running, both the  $X$  and the Higgs can be discovered.

We will first dwell on the discovery of the  $X$  when both of the pair-produced  $X$ s decay to  $Z + j$ . For the purposes of this paper, we will restrict ourselves to looking at leptonic decay modes of the  $Z$  as it has considerably less background, but a full collider study can combine various channels and extend the reach in  $m_X$ .

We will then use the value of  $m_X$  extracted from this analysis in order to discover the Higgs in the events where one of the  $X$ s decays to  $Z + j$  and the other to  $h + j$ . We will focus on a scenario with a moderately heavy Higgs, with a dominant decay mode to  $W^+W^-$ , although discovery of a light Higgs through  $X$  production should be competitive with Higgs production from the SM as well (possibly utilizing the recent search methods involving boosted final states [31, 32]). Once again, we will limit ourselves to leptonic decays of the  $Z$  as well as the  $W$ s, but in a more detailed analysis, several channels can be combined to extend the discovery reach.

Let us start with the Tevatron bounds on  $m_X$ . The strongest constraint arises from a recent analysis of  $WZ$  production [33], searching for events with exactly three final state leptons. In our benchmark model, events with pair-produced  $X$  decaying to  $Z$ ,  $h$  and jets, followed by  $h \rightarrow WW$  can be picked up by this search, as well as  $ZZ$  plus jet final states when both  $Z$  decay leptonically

but one lepton fails to be identified. We implemented the cuts described in Ref. [33], which include requiring the presence of an  $e^+e^-$  or  $\mu^+\mu^-$  pair with invariant mass in the interval [86 GeV, 106 GeV] as well as  $p_{T,\ell_1} > 20 \text{ GeV}$ ,  $p_{T,(\ell_2,\ell_3)} > 10 \text{ GeV}$  and  $\cancel{E}_T > 25 \text{ GeV}$ . We find that for  $m_X > 300 \text{ GeV}$ , the number of events from  $X$  production after the selection cuts falls within one standard deviation of the SM expectation. The  $WW$  final state poses a weaker constraint, because in this final state a veto on hard jets is imposed in order to reduce the  $t\bar{t}$  background [34]. For  $m_X > 300 \text{ GeV}$  the  $X$ -production cross-section is only a fraction of the  $t\bar{t}$  cross-section, so there is no additional constraint from searches for  $t\bar{t}$  either. Finally, for the same range in  $m_X$ , the Higgs production from  $X$  decays is significantly below the SM Higgs production cross-section for the same  $m_h$ , so Higgs searches also do not give additional constraints. In order to stay consistent with these constraints, we will concentrate on the rest of this section on two mass points,  $m_X = 300 \text{ GeV}$  and  $m_X = 550 \text{ GeV}$ , both with  $m_h = 200 \text{ GeV}$ .

In our analysis, we generate  $3 \times 10^5$  parton level events (at 14-TeV LHC running) for each value of  $m_X$  using the user-mode of **MadGraph** [35] and CTEQ6 parton distribution functions [30]. We decay the  $X$ ,  $h$ ,  $W$  and  $Z$  particles using **BRIDGE** [36] in order for the angular distributions of the final-state leptons and jets to be accurate. In the signal sample we allow all possible decays of  $X$ ,  $h$ ,  $W$  and  $Z$  in order to take full account of the combinatoric background, while in the background samples we force leptonic decays (including  $\tau$ 's) since hadronically decaying background events will not pass our selection cuts. The hadronization and detector simulation are done with the **PYTHIA** [37] and **PGS** [21] interface in **MadGraph**, with the default CMS parameter set. This parameter set uses a tracker and muon system  $\eta$  coverage up to 2.4, and a minimum lepton  $p_T$  of 5 GeV. Cone jets with  $\Delta R = 0.5$  are used, note however that our analysis is inclusive and we do not place any cuts on jets. The **PGS** default algorithms are used for lepton isolation as well as other details of detector simulation. As the background for the  $X$  search we generated a matched  $ZZ + \text{jets}$  sample containing 53494 events after matching, using the MLM matching in **MadGraph**, and the same tools as were used for the signal. For the Higgs search we generated a matched  $t\bar{t}Z + \text{jet}$  sample with 36120 events after matching in the same way.

#### 1. Discovering the $X$ .

In order to discover the  $X$ , we focus on the  $ZZ$  final state, where both  $Z$ s decay leptonically. For SM backgrounds, we have generated an MLM-matched sample with  $ZZ$ ,  $ZZ + j$ , and  $ZZ + 2j$ . As our event selection criteria, we demand that an event contains two (distinct)  $Z$  candidates, where a  $Z$  candidate is defined as an  $e^+e^-$  or a  $\mu^+\mu^-$  pair with an invariant mass within

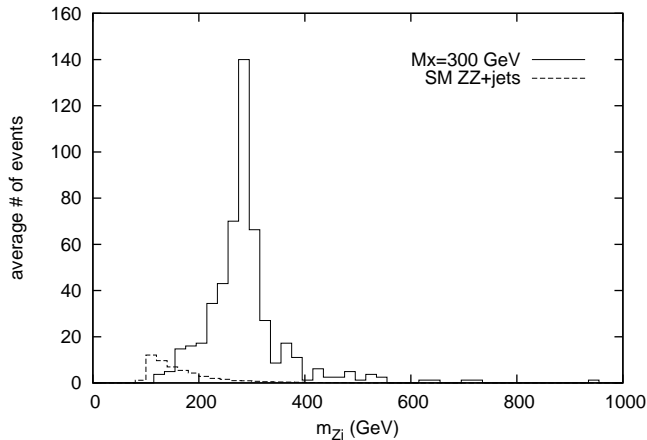


FIG. 11: Distribution of the average  $Z$ +jet pair mass for signal ( $m_X = 300$  GeV) and background in  $10 \text{ fb}^{-1}$  of LHC data (14 TeV).

5 GeV of  $m_Z$ . We then pair the two  $Z$  candidates with the two hardest jets in the event (which in the case of signal are expected to come from the partons of the  $X$  decays) and retain the pairing where the  $Zj$  pair masses are closer to each other. We then plot the average pair mass  $m_{Zj}$ , where the peak from the  $X$  is clearly visible and distinguishable from the  $ZZ + \text{jets}$  background. For  $m_X = 300$  GeV, where the branching fraction  $X \rightarrow Zj$  is 0.76, the cross-section before (after) selection is 36.8 pb (50.5 fb). Similarly, before (after) selection we obtained 1.43 pb (1.32 fb) for  $m_X = 550$  GeV, where the branching fraction  $X \rightarrow Zj$  is 0.57. Leptonic branching fractions and selection cuts reduce the SM background cross section from 11.4 pb down to 5.1 fb. The results for the two mass points and for  $10 \text{ fb}^{-1}$  are plotted in Fig. 11 and Fig. 12. Since the background peaks towards low values of  $m_{Zj}$ , a cut on  $m_{Zj}$  can improve signal significance. For the  $m_X = 550$  GeV case we use  $m_{Zj} \geq 430$  GeV as a selection cut. While a similar cut can also be used for the  $m_X = 300$  GeV case, signal is already much larger than background in this case and therefore a cut on  $m_{Zj}$  is not essential. With this additional cut, the signal cross section becomes 0.85 fb while background is reduced to 0.074 fb. With an integrated luminosity of  $10 \text{ fb}^{-1}$ , this translates to an average 9.2 events with a background expectation of 0.74 events. Using Poisson statistics, this corresponds to a probability of  $9.4 \times 10^{-8}$ , equivalent to more than a  $5\sigma$  upward fluctuation in a Gaussian distribution. We conclude that  $m_X$  up to  $\approx 550$  GeV is discoverable with  $10 \text{ fb}^{-1}$  at  $\sqrt{s} = 14$  TeV.

## 2. Discovering the Higgs

In order to discover the Higgs, we focus on the  $Zh$  final state, where the  $Z$  as well as the  $W$ s from the Higgs decay to leptons. More concretely, our event selection criteria

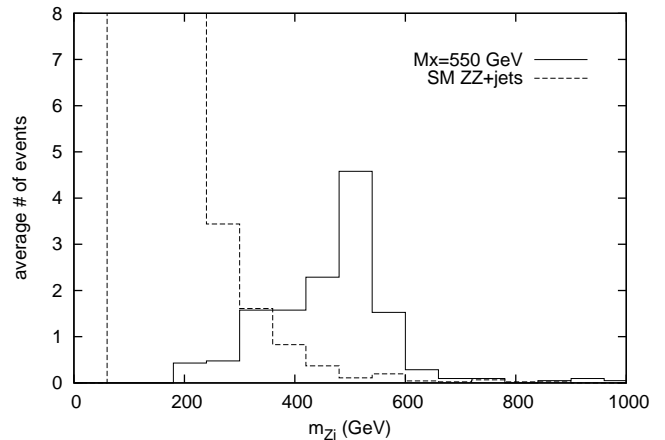


FIG. 12: Distribution of the average  $Z$ +jet pair mass for signal ( $m_X = 550$  GeV) and background in  $10 \text{ fb}^{-1}$  of LHC data (14 TeV).

are:

- The event contains two positively and two negatively charged leptons, with exactly one  $Z$  candidate (as defined above).
- The  $Z$  candidate and (at least) one of the two hardest jets has an invariant mass within 90 GeV of  $m_X$  as determined in the previous section.

For  $m_X = 300$  GeV the selection reduced the signal cross-section from 36.8 pb to 22.2 fb, for  $m_X = 550$  GeV from 1.43 pb to 0.87 fb. With the first selection criterion, the dominant background is  $t\bar{t}Z + \text{jet(s)}$ . At parton level, we generated an MLM-matched sample with up to one extra parton, i.e.,  $t\bar{t}Z$  and  $t\bar{t}Z + j$ . The second selection criterion, which uses the value for  $m_X$  obtained with the search strategy described in the previous subsection, then further reduces the background such that we are essentially left with a pure signal sample. Leptonic branching fractions and the selection cuts reduce the background cross-section from 0.61 pb to 0.40 fb (0.083 fb), applying the two selection criteria for  $m_X = 300$  GeV ( $m_X = 550$  GeV). For both mass points, this corresponds to discovery level statistical significance. Using Poisson statistics in the heavy mass case, the probability for a background fluctuation to mimic the signal is  $2.4 \times 10^{-7}$ , equivalent to more than  $5\sigma$  in a gaussian distribution.

We then identify the two leptons which do not belong to the  $Z$  candidate, and form the transverse mass variable  $M_{T,WW}$  as follows:

$$M_{T,WW}^2 = (E_{T,l+l-} + E_{T,\nu\bar{\nu}})^2 - (\vec{p}_{T,l+l-} + \vec{p}_{T,\text{miss}})^2, \quad (16)$$

where

$$\begin{aligned} E_{T,l+l-}^2 &= p_{T,l+l-}^2 + m_{l+l-}^2, \\ E_{T,\nu\bar{\nu}}^2 &= p_{T,\text{miss}}^2 + m_{l+l-}^2. \end{aligned} \quad (17)$$

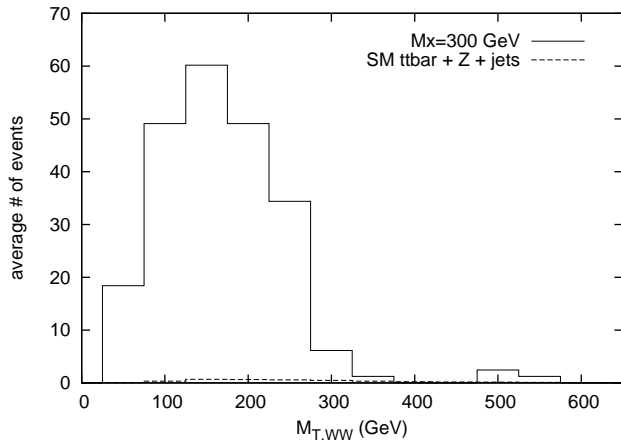


FIG. 13: Distribution of  $M_{T,WW}$  for signal ( $m_X = 300$  GeV,  $m_h = 200$  GeV) and background with a luminosity of  $10 \text{ fb}^{-1}$ .

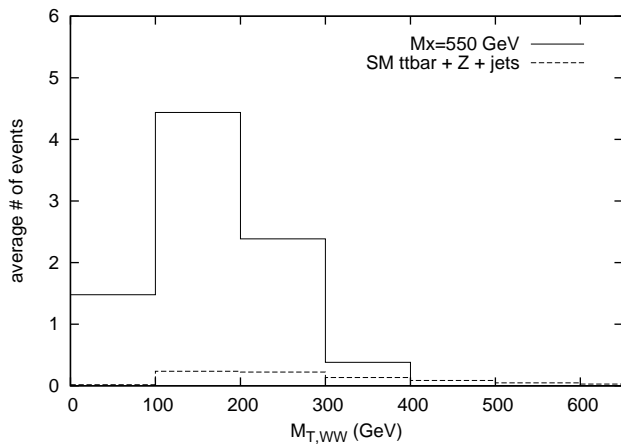


FIG. 14: Distribution of  $M_{T,WW}$  for signal ( $m_X = 550$  GeV,  $m_h = 200$  GeV) and background with a luminosity of  $10 \text{ fb}^{-1}$ .

Note that  $E_{T,\nu\bar{\nu}}$  is only an approximation to the true transverse energy of the neutrino system

$$E_{T,\nu\bar{\nu},\text{true}}^2 = p_{T,\nu\bar{\nu}}^2 + m_{\nu\bar{\nu}}^2. \quad (18)$$

Although this approximation only becomes exact when the  $W$  are produced at threshold, for a 200-GeV Higgs the  $M_{T,WW}$  distribution still peaks near the Higgs mass. We plot the results for the  $m_X = 300$  GeV in Fig. 13 and for  $m_X = 550$  GeV in Fig. 14.

## VI. CONCLUDING REMARKS

The minimal way to incorporate a WIMP DM candidate is as the neutral component of an electroweak triplet with zero hypercharge. We have looked for possible extensions of the SM that contain such a triplet as well as additional matter fields as necessary for gauge coupling

unification. We have identified the characteristic features of such models. New colored particles at the TeV scale are ubiquitous, which can be produced at the LHC. The colored particles allow couplings such that they dominantly decay to a Higgs and a jet, within or outside the LHC detector depending on the size of the couplings. The former possibility gives rise to a new channel for Higgs production, while the latter leads to spectacular R-hadron signals. In order to study these interesting characteristic collider signatures of WIMP DM and unification, we have chosen the model with the simplest matter content as a benchmark. The benchmark model contains two generations of an  $SU(2)_L$ -doublet color-triplet particle  $X$  that decay via Yukawa-type couplings to the SM. In particular, the final states contain  $W$ 's,  $Z$ 's and Higgses, as well as down-type quarks.

We have then investigated the constraints from flavor bounds on the size of the Yukawa-type coupling that leads to the  $X$  decay. We showed that there is a range where the  $X$  can decay promptly, or can be long-lived (stable on collider time scales). We have explored each of these possibilities in turn, showing that in the case of the long-lived  $X$ , R-hadrons can be discovered at the early LHC (7 TeV) up to  $m_X = 650$  GeV, and past 1 TeV with a 14-TeV running.

In the case where the  $X$  particles decay promptly, a large number of Higgs bosons are produced through the decays, which, depending on the  $X$  mass, can be discovered with less luminosity than would be possible from SM Higgs production. We have shown that, for  $m_X \lesssim 550$  GeV and with  $10 \text{ fb}^{-1}$  of data at the LHC, we can discover the  $X$  itself in the leptonic  $ZZ$  final state as well as the Higgs bosons from  $X$  decays in the leptonic  $WW$  final state for a benchmark Higgs mass  $m_h = 200$  GeV.

While in this paper our goal was to focus only on signals that are clean and have little background, these studies can be significantly expanded in a more dedicated collider search. In particular, semi-leptonic decay channels can be combined with the fully leptonic ones to increase the reach. The discovery potential of a light Higgs should be enhanced as well, especially utilizing the recently introduced search methods relying on boosted final states. Finally, models other than the benchmark model we have chosen can be studied for qualitatively different final states. For example, while final states with up-type quarks (in particular the top quark) are rare in the benchmark model, other models can give rise to a large number of tops produced from the decays of the new physics (in addition to the two signals we discussed in this paper). Another interesting problem is to study the case where  $X$  decays within the detector with a displaced vertex or with a macroscopic length. These questions will be further explored in future work.

### Acknowledgments

We thank T. Adams, H. Prosper, and M. Strassler for discussions. We also thank B. Tweedie and Z. Chacko for comments on the manuscript. The work of CK is supported by DOE grant DE-FG02-96ER50959. KK is supported by DOE grant DE-FG02-97ER41022 and the Department of Physics at FSU. TO is supported by a First Year Assistant Professor Award and the Department of Physics at FSU.

### Appendix A: Forbidding proton decay

In Sec. II, we did not require the unification scale to be high enough to suppress proton decay. For example, in the benchmark  $V + 2X$  model, the unification scale is  $M_{\text{GUT}} \sim 10^{11}$  GeV, significantly lower than the standard GUT scale  $\sim 10^{16}$  GeV. Therefore, it is essential to discuss how proton decay can be avoided in principle, even though it has no phenomenological relevance at the TeV scale.

A robust way to avoid the proton decay problem is simply to forbid it by a symmetry. For example, we can consider “baryon triality” [38],  $\phi \rightarrow e^{i\frac{2\pi}{3}(B_\phi - 2Y_\phi)}\phi$ , where  $B_\phi$  and  $Y_\phi$  are the baryon number and hypercharge of a field  $\phi$ , respectively. Baryon triality implies that the baryon number can only be violated in units of 3. Thus, it will absolutely forbid not only proton decay but also neutron-antineutron oscillation [39]. Alternatively, for forbidden proton decay only, one could impose “quark parity”,  $q, d^c, u^c \rightarrow -q, -d^c, -u^c$ .

Clearly, such symmetries necessarily treat quarks and leptons differently, so the simplest possibility of embedding quarks and leptons into unified GUT multiplets (e.g.  $\mathbf{5} \oplus \mathbf{10}$  for SU(5)) does not work. Instead, quarks and leptons must come from separate multiplets, e.g.:

$$\bar{\mathbf{5}}_{d^c} = \begin{pmatrix} d^c \\ 0 \end{pmatrix}, \quad \bar{\mathbf{5}}_\ell = \begin{pmatrix} 0 \\ \ell \end{pmatrix}, \quad (\text{A1})$$

where  $\bar{\mathbf{5}}_{d^c}$  and  $\bar{\mathbf{5}}_\ell$  carry the same baryon triality (or quark parity) quantum numbers as  $d^c$  and  $\ell$ , respectively. Before discussing how to promote such incomplete multiplets to fully GUT-invariant multiplets, we would like to point out that splitting SM matter fields from their heavy “GUT partners” is plausible in the sense that there is already a split multiplet, i.e. the Higgs doublet, and whatever mechanism that splits the Higgs from its GUT partner could also work for the SM matter fields. Moreover, separating quarks and leptons allows us to trivially incorporate non-unified mass relations for the 1st and 2nd generations (i.e.  $m_e/m_d, m_\mu/m_s \neq 1$  at the unification scale).

Now, let us discuss how the above “incomplete” multiplets can be compatible with a GUT symmetry. A simple and plausible way to do so is to copy the mechanism [40] of “incomplete” multiplets nature already has in the

low-energy QCD. QCD undergoes a symmetry breaking from  $G \equiv \text{SU}(3)_L \otimes \text{SU}(3)_R$  down to  $H \equiv \text{SU}(3)_{L \oplus R}$ . Here, the low-mass hadrons form “incomplete” multiplets”, i.e. multiplets of the unbroken subgroup  $H$ , not those of the full group  $G$ . Of course, the theory must be invariant under  $G$ , which is accomplished by nonlinear realization [41] in terms of the Nambu-Goldstone boson field  $\Sigma$  transforming as  $\Sigma \rightarrow g\Sigma h^{-1}$  with  $g \in G$  and  $h \in H$ . This permits us to promote any multiplet of  $H$ ,  $\phi_H$ , to a full multiplet of  $G$ ,  $\phi_G$ , as  $\phi_G \equiv \Sigma\phi_H$ .

By analogy, let us consider the following GUT scenario. Imagine a new confining strong dynamics with a “flavor symmetry”  $G = \text{SU}(5)$  which undergoes “chiral symmetry breaking”  $G \rightarrow H$  with  $H = \text{SU}(3) \otimes \text{SU}(2) \otimes \text{U}(1)$ .  $G$  is also weakly gauged, providing the SM gauge group with a single unified coupling at the  $G$  confinement scale (which therefore can be called the GUT scale). We then imagine that the split quark and lepton multiplets as well as the Higgs doublet are “hadrons” of the new strong dynamics which form multiplets of  $H$ , with appropriate quark parity or baryon triality, etc. They can be promoted to full  $G$  multiplets by nonlinear realization. (If we further integrate in the “ $\rho$  mesons” into this picture by employing “hidden local symmetry” [42], then we essentially obtain the 2-site moose model considered in Ref. [43].)

Constructing an explicit, UV-complete 4D gauge theory that realizes this scenario is beyond the scope of this paper, but it is straightforward to construct a 5D realization via the AdS/CFT correspondence [44], as is done in Ref. [45]. The simplest setup would be the Randall-Sundrum framework [46], i.e., where we take the UV boundary and the bulk to be  $G$ -symmetric while the IR boundary to be only  $H$ -symmetric, by putting a  $G$  gauge field in the bulk with the boundary condition that the  $G/H$  gauge bosons vanish at the IR boundary. The split matter and Higgs multiplets can then be put either in the bulk with the appropriate boundary conditions to project out the unwanted “ $G$ -partner” states, or simply at the IR boundary as multiplets of  $H$ . With an appropriate symmetry such as quark parity or baryon triality, this setup solves the proton decay problem, but since the scale associated with the IR boundary is the GUT scale, there are no observable consequences of the Kaluza-Klein excitations. (There are, however, RS GUT models with the TeV-scale IR brane, with split multiplets and a discrete symmetry to forbid proton decay, which do have experimental consequences at the TeV scale [47]. The main difference between those models and ours is that their physics above the TeV scale is a strong conformal dynamics (or a 5D theory via AdS/CFT) while we assume a perturbative 4D physics up to the GUT scale.)

### Appendix B: Effects of higher-dimensional operators

Here we would like to show that adding nonrenormalizable interactions to our Lagrangian (1) does not alter



our results. In particular, one might worry that a higher-dimensional operator might lead to a prompt decay of the  $X$  even when  $\lambda = 0$ , destroying the R-hadron scenario. Fortunately, this is not the case. The leading nonrenormalizable interaction that can let  $X$  decay is

$$\frac{1}{\Lambda}(X^c H^*)(qH^*), \quad (\text{B1})$$

where  $\Lambda$  is some high scale. By our assumption, there is no new threshold between the TeV scale and the unification scale, so  $\Lambda$  must be at least  $\sim 10^{11}$  GeV. To avoid a suppression from three-body phase space, one of the Higgs fields can be put to its VEV. Therefore, the  $X$

decay length due to this operator is at least

$$\Gamma^{-1} \sim \left[ \frac{m_X v^2}{16\pi(10^{11} \text{ GeV})^2} \right]^{-1} \simeq 3 \text{ m} \frac{1 \text{ TeV}}{m_X}. \quad (\text{B2})$$

Thus even the most conservative estimate gives a decay length comparable to the dimensions of the LHC detectors. Therefore, higher-dimensional operators do not upset our conclusions. Since this  $X$  decay is still prompt on a cosmological time scale, setting  $\lambda = 0$  in the coupling (4) is actually allowed cosmologically, as  $X$  can decay via the above operator.

- 
- [1] D. S. Akerib *et al.* [CDMS Collaboration], Phys. Rev. Lett. **96** (2006) 011302 [arXiv:astro-ph/0509259].
- [2] M. Cirelli, A. Strumia and M. Tamburini, Nucl. Phys. B **787** (2007) 152 [arXiv:0706.4071 [hep-ph]].
- [3] H. Georgi and S. L. Glashow, Phys. Rev. Lett. **32** (1974) 438; H. Georgi, H. R. Quinn and S. Weinberg, Phys. Rev. Lett. **33** (1974) 451.
- [4] N. Arkani-Hamed and S. Dimopoulos, JHEP **0506** (2005) 073 [arXiv:hep-th/0405159].
- [5] G. F. Giudice and A. Romanino, Nucl. Phys. B **699** (2004) 65 [arXiv:hep-ph/0406088].
- [6] J. Erler and P. Langacker, Phys. Rev. Lett. **105** (2010) 031801 [arXiv:1003.3211 [hep-ph]]; O. Eberhardt, A. Lenz and J. Rohrwild, arXiv:1005.3505 [hep-ph].
- [7] K. Nakamura *et al.* (Particle Data Group), Journal of Physics G **37**, 075021 (2010).
- [8] J. Thaler and L. T. Wang, JHEP **0807** (2008) 092 [arXiv:0806.0023 [hep-ph]]; D. E. Kaplan, K. Rehermann, M. D. Schwartz and B. Tweedie, Phys. Rev. Lett. **101** (2008) 142001 [arXiv:0806.0848 [hep-ph]]; L. G. Almeida, S. J. Lee, G. Perez, I. Sung and J. Virzi, Phys. Rev. D **79** (2009) 074012 [arXiv:0810.0934 [hep-ph]]; T. Plehn, M. Spannowsky, M. Takeuchi and D. Zerwas, arXiv:1006.2833 [hep-ph]; K. Rehermann and B. Tweedie, arXiv:1007.2221 [hep-ph].
- [9] D. Choudhury, T. M. P. Tait and C. E. M. Wagner, Phys. Rev. D **65** (2002) 053002 [arXiv:hep-ph/0109097]; K. Kumar, W. Shepherd, T. M. P. Tait and R. Vega-Morales, arXiv:1004.4895 [hep-ph].
- [10] C. Csaki, A. Falkowski and A. Weiler, JHEP **0809** (2008) 008 [arXiv:0804.1954 [hep-ph]]; G. Isidori, Y. Nir and G. Perez, [arXiv:1002.0900 [hep-ph]].
- [11] G. D'Ambrosio, G. F. Giudice, G. Isidori and A. Strumia, Nucl. Phys. B **645** (2002) 155 [arXiv:hep-ph/0207036].
- [12] T. Hurth, G. Isidori, J. F. Kamenik and F. Mescia, Nucl. Phys. B **808** (2009) 326 [arXiv:0807.5039 [hep-ph]].
- [13] R. Barbieri, A. Pomarol, R. Rattazzi and A. Strumia, Nucl. Phys. B **703** (2004) 127 [arXiv:hep-ph/0405040].
- [14] S. Dimopoulos, M. Dine, S. Raby and S. D. Thomas, Phys. Rev. Lett. **76** (1996) 3494 [arXiv:hep-ph/9601367]; K. T. Matchev and S. D. Thomas, Phys. Rev. D **62** (2000) 077702 [arXiv:hep-ph/9908482]; N. Arkani-Hamed and S. Dimopoulos, JHEP **0506** (2005) 073 [arXiv:hep-th/0405159]; S. P. Martin, Phys. Rev. D **62** (2000) 095008 [arXiv:hep-ph/0005116].
- [15] Z. Chacko, C. A. Krenke and T. Okui, JHEP **0901** (2009) 050 [arXiv:0809.3820 [hep-ph]].
- [16] M. J. Strassler and K. M. Zurek, Phys. Lett. B **651** (2007) 374 [arXiv:hep-ph/0604261]; M. J. Strassler and K. M. Zurek, Phys. Lett. B **661** (2008) 263 [arXiv:hep-ph/0605193]; J. E. Juknevich, D. Melnikov and M. J. Strassler, JHEP **0907** (2009) 055 [arXiv:0903.0883 [hep-ph]].
- [17] J. Kang and M. A. Luty, JHEP **0911** (2009) 065 [arXiv:0805.4642 [hep-ph]].
- [18] C. Kilic, T. Okui and R. Sundrum, JHEP **1002** (2010) 018 [arXiv:0906.0577 [hep-ph]]; C. Kilic and T. Okui, JHEP **1004** (2010) 128 [arXiv:1001.4526 [hep-ph]]; Y. Bai and R. J. Hill, arXiv:1005.0008 [hep-ph].
- [19] G. Brooijmans *et al.*, arXiv:1005.1229 [hep-ph].
- [20] P. Meade, M. Reece and D. Shih, arXiv:1006.4550 [hep-ph].
- [21] J. Conway *et al.*, <http://www.physics.ucdavis.edu/~conway/research/software/pgs/pgs4-general.htm>.
- [22] A. Arvanitaki, S. Dimopoulos, A. Pierce, S. Rajendran and J. G. Wacker, Phys. Rev. D **76** (2007) 055007 [arXiv:hep-ph/0506242].
- [23] M. Cirelli, N. Fornengo and A. Strumia, Nucl. Phys. B **753** (2006) 178 [arXiv:hep-ph/0512090].
- [24] A. C. Kraan, J. B. Hansen and P. Nevski, Eur. Phys. J. C **49** (2007) 623 [arXiv:hep-ex/0511014].
- [25] A. C. Kraan, Eur. Phys. J. C **37** (2004) 91 [arXiv:hep-ex/0404001].
- [26] T. Aaltonen *et al.* [CDF Collaboration], Phys. Rev. Lett. **103** (2009) 021802 [arXiv:0902.1266 [hep-ex]].
- [27] V. M. Abazov *et al.* [D0 Collaboration], Phys. Rev. Lett. **102**, 161802 (2009) [arXiv:0809.4472 [hep-ex]].
- [28] T. Adams, private communication.
- [29] A. Pukhov *et al.*, arXiv:hep-ph/9908288; A. Pukhov, arXiv:hep-ph/0412191.
- [30] J. Pumplin, D. R. Stump, J. Huston, H. L. Lai, P. M. Nadolsky and W. K. Tung, JHEP **0207** (2002) 012 [arXiv:hep-ph/0201195].
- [31] J. M. Butterworth, A. R. Davison, M. Rubin and G. P. Salam, Phys. Rev. Lett. **100** (2008) 242001 [arXiv:0802.2470 [hep-ph]]; T. Plehn, G. P. Salam and M. Spannowsky, Phys. Rev. Lett. **104** (2010) 111801 [arXiv:0910.5472 [hep-ph]]; G. D. Kribs, A. Martin, T. S. Roy and M. Spannowsky, Phys. Rev. D **81** (2010) 111501 [arXiv:0912.4731 [hep-ph]].

- D. E. Soper and M. Spannowsky, arXiv:1005.0417 [hep-ph]; G. D. Kribs, A. Martin, T. S. Roy and M. Spannowsky, arXiv:1006.1656 [hep-ph].
- [32] D. Krohn, J. Thaler and L. T. Wang, JHEP **0906** (2009) 059 [arXiv:0903.0392 [hep-ph]]; S. D. Ellis, C. K. Vermilion and J. R. Walsh, Phys. Rev. D **80** (2009) 051501 [arXiv:0903.5081 [hep-ph]]; S. D. Ellis, C. K. Vermilion and J. R. Walsh, Phys. Rev. D **81** (2010) 094023 [arXiv:0912.0033 [hep-ph]]; D. Krohn, J. Thaler and L. T. Wang, JHEP **1002** (2010) 084 [arXiv:0912.1342 [hep-ph]].
- [33] V. M. Abazov *et al.* [D0 Collaboration], arXiv:1006.0761 [hep-ex]; [CDF Collaboration], (CDF note 10176).
- [34] V. M. Abazov *et al.* [D0 Collaboration], Phys. Rev. Lett. **103** (2009) 191801 [arXiv:0904.0673 [hep-ex]]; T. Aaltonen *et al.* [CDF Collaboration], Phys. Rev. Lett. **104**, 201801 (2010) [arXiv:0912.4500 [hep-ex]].
- [35] J. Alwall *et al.*, JHEP **0709**, 028 (2007) [arXiv:0706.2334 [hep-ph]].
- [36] P. Meade and M. Reece, arXiv:hep-ph/0703031.
- [37] T. Sjostrand, S. Mrenna and P. Z. Skands, JHEP **0605**, 026 (2006) [arXiv:hep-ph/0603175].
- [38] L. E. Ibanez and G. G. Ross, Nucl. Phys. B **368** (1992) 3.
- [39] D. J. Castano and S. P. Martin, Phys. Lett. B **340** (1994) 67 [arXiv:hep-ph/9408230].
- [40] K. Inoue, A. Kakuto and H. Takano, Prog. Theor. Phys. **75** (1986) 664; A. A. Anselm and A. A. Johansen, Phys. Lett. B **200** (1988) 331; R. Barbieri, G. R. Dvali and A. Strumia, Nucl. Phys. B **391** (1993) 487.
- [41] S. R. Coleman, J. Wess and B. Zumino, Phys. Rev. **177** (1969) 2239; C. G. Callan, S. R. Coleman, J. Wess and B. Zumino, Phys. Rev. **177** (1969) 2247.
- [42] M. Bando, T. Kugo, S. Uehara, K. Yamawaki and T. Yanagida, Phys. Rev. Lett. **54** (1985) 1215.
- [43] N. Weiner, arXiv:hep-ph/0106097.
- [44] For reviews, see O. Aharony, S. S. Gubser, J. M. Maldacena, H. Ooguri and Y. Oz, Phys. Rept. **323**, 183 (2000) [arXiv:hep-th/9905111] and T. Gherghetta, Les Houches lectures 2005, in “Particle physics beyond the standard model,” Les Houches 2005, 263-311 [arXiv:hep-ph/0601213].
- [45] Y. Nomura, D. Poland and B. Tweedie, JHEP **0612** (2006) 002 [arXiv:hep-ph/0605014].
- [46] L. Randall and R. Sundrum, Phys. Rev. Lett. **83** (1999) 3370 [arXiv:hep-ph/9905221].
- [47] K. Agashe and G. Servant, Phys. Rev. Lett. **93** (2004) 231805 [arXiv:hep-ph/0403143]; K. Agashe and G. Servant, JCAP **0502** (2005) 002 [arXiv:hep-ph/0411254].